

Multi-Parametric Relationships between PAM Measurements and Carbon Incorporation, an *In Situ* Approach

Camille Napoléon^{1,2,3}, Pascal Claquin^{1,2*}

1 Université de Caen Basse-Normandie, BIOMEA FRE3484 CNRS, Caen, France, **2** CNRS INEE, FRE3484 BIOMEA, Caen, France, **3** IFREMER, Laboratoire Environnement Ressources de Normandie, Avenue du Général de Gaulle, Port-en-Bessin, France

Abstract

Primary production (PP) in the English Channel was measured using ¹³C uptake and compared to the electron transport rate (ETR) measured using PAM (pulse amplitude modulated fluorometer). The relationship between carbon incorporation (P_{obs}) and ETR was not linear but logarithmic. This result can be explained by alternative electron sinks at high irradiance which protect the phytoplankton from photoinhibition. A multi-parametric model was developed to estimate PP by ETR. This approach highlighted the importance of taking physicochemical parameters like incident light and nutrient concentrations into account. The variation in the ETR/ P_{obs} ratio as a function of the light revealed different trends which were characterized by three parameters (R_{max} , the maximum value of ETR/ P_{obs} ; E_{Rmax} , the light intensity at which R_{max} is measured; γ the initial slope of the curve). Based on the values of these three parameters, data were divided into six groups which were highly dependent on the seasons and on the physicochemical conditions. Using the multi-parametric model which we defined by P_{obs} and ETR measurements at low frequencies, the high frequency measurements of ETR enabled us to estimate the primary production capacity between November 2009 and December 2010 at high temporal and spatial scales.

Citation: Napoléon C, Claquin P (2012) Multi-Parametric Relationships between PAM Measurements and Carbon Incorporation, an *In Situ* Approach. PLoS ONE 7(7): e40284. doi:10.1371/journal.pone.0040284

Editor: Terence Evens, US Dept. of Agriculture – Agricultural Research Service (USDA-ARS), United States of America

Received: January 31, 2012; **Accepted:** June 4, 2012; **Published:** July 20, 2012

Copyright: © 2012 Napoléon, Claquin. This is an open-access article distributed under the terms of the Creative Commons Attribution License, which permits unrestricted use, distribution, and reproduction in any medium, provided the original author and source are credited.

Funding: This study was supported by the European project Interreg 4a Channel integrated Approach for marine Resource 3 (CHARM 3). The funder had no role in study design, data collection and analysis, decision to publish, or preparation of the manuscript.

Competing Interests: The authors have declared that no competing interests exist.

* E-mail: pascal.claquin@unicaen.fr

Introduction

Primary production forms the base of the marine food web. Consequently, every trophic level depends on it [1] and a reliable estimation of primary production is indispensable for understanding and creating models of marine ecosystems. However, numerous environmental factors control the dynamics of primary production [2,3], which makes its estimation difficult.

Remote sensing is commonly used to estimate primary production by using stock data of chlorophyll *a* [4,5,6] but results have rarely been validated by *in situ* measurements. Grangeré et al. [7] showed underestimation of primary production by using chlorophyll *a* data. To obtain a precise estimation of primary production, *in situ* measurements are essential. Different methods can be used to make *in situ* measurements of primary production, each of which has advantages and disadvantages. One such method is labelled carbon incorporation [8,9]. This method is sensitive but cannot be used for measurements at large spatio-temporal scales due to its long incubation period. Yet the study of the spatiotemporal dynamics of primary production requires data at large spatiotemporal scales. The PAM (pulse amplitude modulated fluorometer) method based on the variation in chlorophyll *a* fluorescence in the Photosystem II is more flexible as it allows rapid measurements of photosynthetic parameters and estimates the physiological state of the phytoplankton [10,11]. This in turn, means that phytoplankton productivity can be monitored

at large spatial and temporal scales. In addition, PAM is sensitive and non-invasive.

The labelled carbon incorporation method enables the incorporation of dissolved inorganic carbon into organic matter to be measured whereas the PAM method does not give the rate of photosynthetic carbon incorporation directly [12,13] but enables access to the electrons transport rate (ETR) from the PSII. Combining these two approaches results in a very powerful tool to estimate carbon assimilation at large spatial and temporal scales. By combining the fluorescence approach and traditional incubation methods, it is possible to estimate the potential production of carbon knowing the electrons flux [12,14,15]. But this relation is not trivial. Environmental factors do not all affect ETR in the same way, so carbon fixation and therefore the number of electrons required to fix one mol of carbon is not constant. For example, the maximum quantum yield of carbon fixation varies as a function of the nitrate concentration [16] or temperature [17]. Various physiological processes can hinder the flow of electrons among others, the Mehler reaction, chlororespiration, photorespiration, and nitrate fixation [12,18,19], in response to environmental changes or as function of the species composition [20].

Many studies have shown that it is possible to use the fluorescence approach by comparing it to other traditional incubation methods to estimate primary production such as labelled carbon incorporation or oxygen measurements [10,12,17,21,22]. By contrast, only a few authors have analysed

the effect of physicochemical [16] or biological parameters [14] on the conversion of photosynthetic electron transport rates (ETR) into carbon fixation rates.

In the present study, we investigated the ETR and ^{13}C incorporation relationships over one year on a transect in the central English Channel [23]. The objectives of the present study were to: i) describe the influence of physicochemical and biological parameters on the relationship between the PAM method and the carbon incubation method, ii) estimate the rate of carbon fixation as a function of ETR using a multi-parametric approach which allows the influence of physicochemical and biological parameters to be taken into account, and to hierarchize them, iii) apply the relationship obtained between carbon fixation rate and ETR on the whole PAM dataset measured at high frequency in the central English Channel between November 2009 and December 2010 [23].

Materials and Methods

1. Study Area

As described in Napoléon et al. [23], measurements were made every month from November 2009 to December 2010 in the central part of the English Channel. The English Channel in North-West Europe is an epicontinental sea which is connected to the North Sea in the north and influenced by the Atlantic Ocean in the west. Napoléon et al. [23] characterised different areas in the central part of the English Channel, revealing that their functioning differed depending on freshwater inputs from rivers or on the influence of offshore water. These different hydrographic conditions drive the dynamics of photosynthetic parameters. Consequently, it is interesting to study primary production in this complex system which comprises both rich and depleted areas.

Data were collected onboard the *Normandie-Brittany ferries* at a depth of four metres during the ferry's daily cruises on a 175 kilometres transect between Ouistreham (France, $49^{\circ}17'27\text{ N}$, $000^{\circ}14'45\text{ W}$) and Portsmouth (Great Britain, $50^{\circ}48'49\text{ N}$, $001^{\circ}05'29\text{ W}$) (Figure 1). Parameters were recorded at the 10 stations shown on the map in Figure 1.

2. Physicochemical Parameters

As described in detail in Napoléon et al. [23], temperature and salinity were recorded with an YSI 6600 V2 multi-parameter probe, and light was measured on the deck with a 2π PAR sensor LI-192 connected to a data Logger LI-1400 (LI-COR, Lincoln, Nebraska, USA). Dissolved inorganic nitrogen (DIN), phosphate (DIP) and silicate (DSi) concentrations were determined in the laboratory using a AA3 auto analyser (AXFLOW) following the method of Aminot and K  rouel [24]. Suspended particulate matter (SPM) was measured following the method of Aminot and Chaussepied [25].

3. Biological Parameters

The chlorophyll *a* (Chl*a*) concentration was measured according to the method of Welschmeyer [26] as described in Napoléon et al. [23]. Phytoplankton were identified in water samples preserved by Lugol's solution (2 mL L^{-1}) using the Uterm  hl method. The dinoflagellate:diatom ratio was calculated for each sample.

To obtain the chlorophyll-specific absorption cross section (a^* ; $\text{m}^2\text{ mg Chl}a^{-1}$), one litre of seawater was filtered onto a GF/F glass-fibre filter. The *in vivo* optical density of total particles (OD_t) from 400 to 750 nm was measured directly on the filter using a Perkin Elmer integrating sphere spectrophotometer [27]. The sample was recovered with methyl alcohol (MeOH) to extract phytoplankton pigments [28]. After one hour, the *in vivo* optical density for non-algal particles (OD_{np}) was measured directly on the filter rinsed with filtered seawater. The optical density of the phytoplankton (OD_p) was determined using:

$$OD_p(\lambda) = OD_t(\lambda) - OD_{np}(\lambda) \quad (1)$$

The chlorophyll-specific absorption cross section (a^* ; $\text{m}^2\text{ mg Chl}a^{-1}$) was calculated using the equation of Johnsen and Sakshaug [29]:

$$a^* = (A * S * 2.3) / (V * [Chl a]) \quad (2)$$

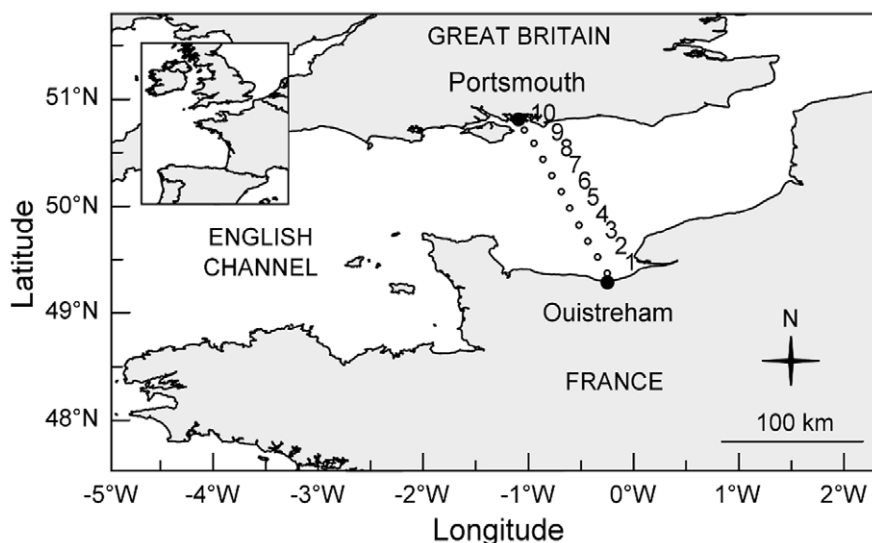


Figure 1. Map of the sampling area.

doi:10.1371/journal.pone.0040284.g001

where A is the average OD_p between 400 nm and 700 nm, S is the clearance area of the filter (1256 mm²), V is the filtered volume in mL and the chlorophyll a concentration is in mg m⁻³. a_{ph} in m⁻³ was determined according to [30]:

$$a_{ph} = a^* * [Chla] \quad (3)$$

where the chlorophyll a concentration is in mg m⁻³.

4. PAM Fluorometry

The maximum energy conversion efficiency, or quantum efficiency of PSII charge separation (F_v/F_m) was measured using the flow-through (FT) version of WATER PAM (Walz, Effeltrich, Germany) [31]. As described in Napoléon et al. [23], the water collected at a depth of 4 m was conducted through a pipe to a 100 mL dark tank. After 10 min of dark acclimation, a 30 mL sub-sample was automatically transferred into the measuring chamber. The sample was excited by a weak blue light (1 μ mol photons m⁻² s⁻¹, 470 nm, frequency 0.6 kHz) to record the minimal fluorescence (F_0). The maximum fluorescence (F_m) was obtained during a saturating light pulse (0.6 s, 1700 μ mol photons m⁻² s⁻¹, 470 nm), allowing the quinone A (QA) pool to be reduced. F_v/F_m was calculated according to the following equation [32] after subtraction of the blank fluorescence, measured on seawater filtrated through GF/F glass-fibre filter:

$$F_v/F_m = (F_m - F_0)/F_m \quad (4)$$

The samples were exposed to nine irradiances (E) from 0 to 1000 μ mol photons m⁻² s⁻¹ for 55 s at each step. Steady state fluorescence (F_s) and maximum fluorescence (F_m') were measured. The effective quantum efficiency of PSII for each irradiance was determined as follows [32]:

$$\Delta F/F_m' = (F_m' - F_s)/F_m' \quad (5)$$

The relative electron transport rate (rETR, relative unit) was calculated for each irradiance. rETR is a measure of the rate of linear electron transport through Photosystem II, which is correlated with the overall photosynthetic performance of the phytoplankton [33]:

$$rETR(E) = \Delta F/F_m' * E \quad (6)$$

The electron transport rate (ETR) in μ mol electron L⁻¹ h⁻¹ was calculated as follows:

$$ETR(E) = rETR(E) * a_{ph} * 0.757 * (3600/1000) \quad (7)$$

where a_{ph} is in m⁻³. According to Johnsen and Sakshaug [29] and knowing the species composition, which was largely dominated by diatoms and Dinophyta (data not shown), we assumed that 75.7% of the absorbed photons were allocated to photoreactions in the PSII.

5. ¹³C Incubation

Twenty-two ¹³C incubation experiments were conducted (see Table 1 for dates and stations). A photosynthetic chamber (modified from Babin et al., [8]) was used to perform *in situ* incubations. A U-

shaped dimmable fluorescent tube (OSRAM, DULUX L, 2G11, 55W/12-950, LUMILUX DE LUXE, daylight) produced the light, and the temperature in the photosynthetic chamber was maintained at the *in situ* temperature by a seawater circuit. Immediately after sampling, six litres of seawater were inoculated with NaH¹³CO₃ (98 atom %, Sigma) corresponding to an enrichment of about 15% of the dissolved inorganic carbon already present in the seawater. The inoculated seawater was shared among 20 culture flasks (265 mL) placed in the photosynthetic chamber. Light intensity was measured in each flask using a micro-spherical quantum sensor (US-SQS; Walz) connected to a LI-COR 1400 data logger, and one flask was maintained in the dark to estimate the non-photosynthetic inorganic carbon incorporation. After three hours of incubation, each flask was filtered onto 25 mm pre-combusted (450°C, 12 h) GF/F filters and stored at -20°C until analysis. To remove carbonates, filters were exposed to fuming HCl for four hours and then dried at 50°C for 12 hours. The particulate organic carbon (POC) concentration and the isotopic ratio of ¹³C to ¹²C were determined using an elemental analyzer (EA 3000, Eurovector) combined with a mass spectrophotometer (IsoPrime, Elementar). The carbon fixation rate (P_{obs}) was calculated according to Hama et al. [34]. The value for incorporation in the dark was subtracted from all data and P_{obs} was expressed in μ mol C L⁻¹ h⁻¹. Each P_{obs} vs. E curve was then performed on 20 values.

6. P vs. E Curve

The ETR and P_{obs} were plotted against light (E). To estimate photosynthetic parameters, the mechanistic model of Eilers and

Table 1. R_{max} , E_{Rmax} and γ values per date and station.

Date	Station	R_{Max}	E_{Rmax}	γ
13-Mar-10	4	85.54	349	0.152
13-Mar-10	5	63.17	0	-0.097
5-May-10	3	24.37	876	0.040
5-May-10	5	49.13	4143	0.055
5-May-10	7	10.74	422	0.036
2-Jun-10	3	26.87	394	0.079
2-Jun-10	6	15.31	590	0.040
2-Jun-10	9	4.70	405	0.013
7-Jul-10	4	6.99	368	0.019
7-Jul-10	7	2.54	210	0.013
7-Jul-10	9	5.91	205	0.030
20-Aug-10	4	11.61	143	0.005
20-Aug-10	7	5.49	14	-0.004
20-Aug-10	9	10.09	238	0.016
29-Sep-10	4	21.32	0	-0.024
29-Sep-10	7	7.14	222	0.028
29-Sep-10	9	5.80	328	0.012
22-Oct-10	4	10.38	0	-0.007
22-Oct-10	7	6.58	0	-0.002
22-Oct-10	9	8.66	297	0.018
7-Dec-10	4	10.01	83	-0.003
7-Dec-10	7	8.89	192	0.025

R_{max} is in mol e⁻ mol C⁻¹, E_{Rmax} is in μ mol photons m⁻² s⁻¹ and γ is in mol e⁻ mol C⁻¹ (μ mol photons m⁻² s⁻¹)⁻¹.
doi:10.1371/journal.pone.0040284.t001

Peeter [35] was applied to the data:

$$X(E) = E/(aE^2 + bE + c) \quad (8)$$

where $X(E)$ is ETR (E) or $P_{\text{obs}}(E)$. The maximum photosynthetic capacity was calculated as follows:

$$X_{\text{max}} = 1/(b + 2\sqrt{ac}) \quad (9)$$

where X_{max} is the maximum photosynthetic capacity measured with the PAM method (ETR_{max} in $\mu\text{mol electrons L}^{-1} \text{h}^{-1}$) or with the ^{13}C incubation method (P_{max} in $\mu\text{mol C L}^{-1} \text{h}^{-1}$).

The ETR/ P_{obs} ratio was plotted against light intensity. As a consequence of the use of the mechanistic model of Eilers and Peeter [35] to fit the data, we were able to estimate the relationship between ETR/ P_{obs} and light for each curve by:

$$\text{ETR}(E)/P_{\text{obs}}(E) = (a'E^2 + b'E + c')/(a''E^2 + b''E + c'') \quad (10)$$

Where a' , b' and c' are the estimated parameters of the mechanistic model of Eilers and Peeter [35] for the ETR vs. light relationship and a'' , b'' and c'' for the P_{obs} vs. light relationship.

Three parameters were defined to describe the relationship between ETR/ P_{obs} and light intensity (Figure 2): R_{max} , the maximum value of ETR/ P_{obs} in $\text{mol e}^- \text{mol C}^{-1}$; $E_{R_{\text{max}}}$, the light intensity at which R_{max} was measured in $\mu\text{mol photons m}^{-2} \text{s}^{-1}$; γ , the initial slope of the curve in $\text{mol e}^- \text{mol C}^{-1} (\mu\text{mol photons m}^{-2} \text{s}^{-1})^{-1}$. A Ward's clustering was performed on the three parameters to identify data with the same shaped curve.

The relationships between the shapes of the ETR/ P_{obs} vs. light and physicochemical and biological parameters were examined by principal component analysis (PCA) (software R 2.11.1).

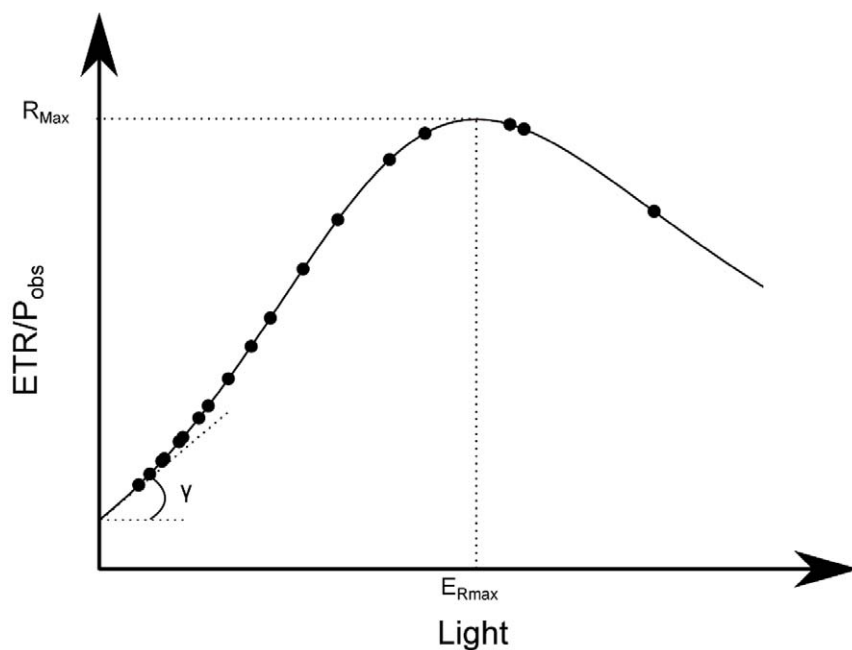


Figure 2. Example of relationship between ETR/ P_{obs} ratio and light. R_{max} is the maximum value of ETR/ P_{obs} , $E_{R_{\text{max}}}$ is the light intensity at which R_{max} is measured and γ the initial slope of the curve. doi:10.1371/journal.pone.0040284.g002

7. Data Analyses

Logarithmic regression analysis was carried out on the full dataset to study the relationship between P_{obs} and ETR using SigmaPlot 11.0 (Systat Software). The logarithmic relationship obtained gave us a model, Sim_{ETR1} , which enabled us to estimate the rate of carbon fixation (P_{simETR1}) using ETR data.

To improve the first Sim_{ETR1} model, the differences between P_{obs} and P_{simETR1} were calculated. Linear dependences between physicochemical and biological parameters and $P_{\text{obs}}-P_{\text{simETR1}}$ (ΔP) were carried out using the Pearson product moment correlation of SigmaPlot 11.0 (Systat Software) to identify the parameters that influenced the relationship between the rate of carbon fixation and ETR. After electing the parameters using the method of forward stepwise regression, a multiple linear regression was performed to estimate ΔP (SigmaPlot 11.0). This estimation was added to Sim_{ETR1} to form Sim_{ETR2} .

Linear regression analyses were performed between P_{obs} and models (Sim_{ETR1} and Sim_{ETR2}) to estimate the significance of these relationships.

Results

1. Carbon Incorporation Estimation Versus ETR

To investigate the relationship between the carbon incorporation and the ETR measurements for our data set measured in the English Channel, we plotted the carbon incorporation observation (P_{obs}), estimated using ^{13}C , against ETR (Figure 3). A significant linear relationship was found between P_{obs} and ETR up to $2 \mu\text{mol e}^- \text{L}^{-1} \text{h}^{-1}$ ($R^2 = 0.4022$, $P_{\text{obs}} = 0.138 * \text{ETR}$, $p < 0.001$). After this point, the relationship was no longer linear and P_{obs} values tended to level off at high ETR values. Consequently, this relationship can be described by a logarithmic function and the dataset was therefore fitted to a two-parameter logarithm curve (Figure 3). Using the logarithm curve, a significant fit ($p < 0.0001$, $P_{\text{obs}} = 0.1503 + 0.0496 * \ln(\text{ETR})$, equation 11) was obtained with a relatively high R^2 value (0.3388).

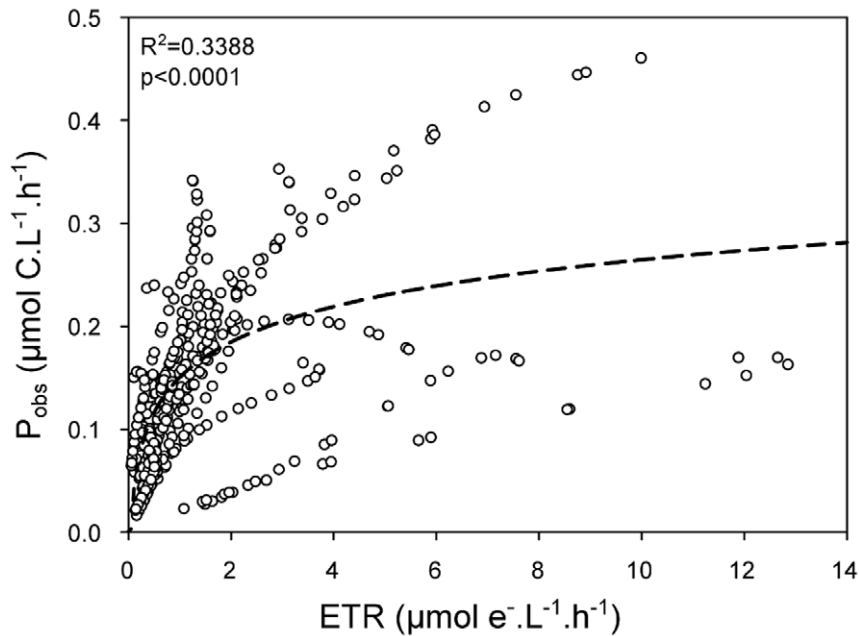


Figure 3. Observed ^{13}C incorporation (P_{obs}) plotted against the electron transport rate (ETR). The dotted line represents the logarithm regression ($P_{\text{obs}} = 0.1503 + 0.0496 * \ln(\text{ETR})$). doi:10.1371/journal.pone.0040284.g003

With a view to estimating PP by ETR, the rate of carbon incorporation was calculated by transforming ETR data with equation 11 determined by the logarithm regression. P_{obs} and our first estimation of carbon incorporation (Sim_{ETR1} , $P_{simETR1} = 0.1503 + 0.0496 * \ln(\text{ETR})$, equivalent to equation 11), was in relatively good agreement ($R^2 = 0.338$, $p < 0.0001$) (Figure 4).

To highlight the physicochemical and biological parameters which drive the relationship between PP and ETR, and to improve the estimation of PP by using ETR, the correlation coefficients of the difference between P_{obs} and $P_{simETR1}$ (ΔP) and physicochemical and biological parameters were calculated (Table 2). High negative correlation coefficients were obtained between ΔP and nutrient concentrations ($r_{\Delta P, \text{DIP}} = -0.701$, $r_{\Delta P, \text{DIN}} = -0.488$, $r_{\Delta P, \text{DSi}} = -0.422$). ΔP was also highly nega-

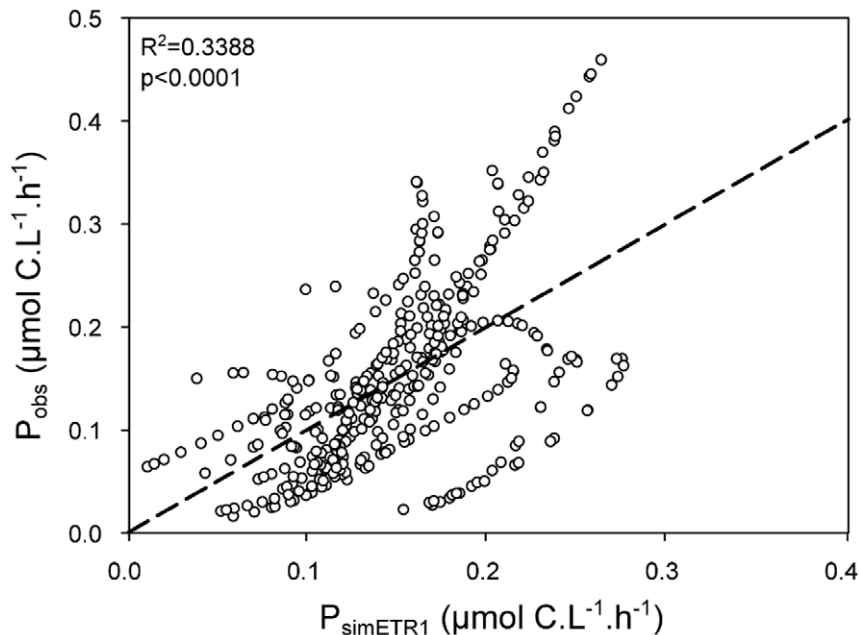


Figure 4. Observed ^{13}C incorporation (P_{obs}) plotted against estimated carbon incorporation by the equation Sim_{ETR1} . $P_{simETR1} = 0.1503 + 0.0496 * \ln(\text{ETR})$. The dotted line represents the linear regression ($P_{\text{obs}} = 1 * P_{simETR1}$). doi:10.1371/journal.pone.0040284.g004

Table 2. Linear correlation coefficients (Pearson) between ΔP and physicochemical and biological parameters.

Parameters	PAR	Temp	DIP	DIN	DSi	Chla	SPM	F _v /F _m	Dino/Diat
ΔP	0.386	0.351	-0.701	-0.488	-0.422	0.250	0.104	-0.475	0.046

PAR: incident light in $\mu\text{mol photons m}^{-2} \text{ s}^{-1}$, Temp: temperature in $^{\circ}\text{C}$, DIP concentrations in $\mu\text{mol L}^{-1}$, DIN concentrations in $\mu\text{mol L}^{-1}$, DSi concentrations in $\mu\text{mol L}^{-1}$, Chla biomass in $\mu\text{g L}^{-1}$, SPM concentrations in mg L^{-1} and F_v/F_m, and dinoflagellate:diatom ratio.
doi:10.1371/journal.pone.0040284.t002

tively correlated with F_v/F_m ($r_{\Delta P, F_v/F_m} = -0.475$) and positively with irradiance ($r_{\Delta P, PAR} = 0.386$). However there were also low correlations between ΔP and the Chla concentration ($r_{\Delta P, Chla} = 0.250$) and the SPM concentration ($r_{\Delta P, SPM} = 0.104$) and no correlation with the dinoflagellate:diatom ratio ($r_{\Delta P, Dino/Diat} = 0.046$).

Parameters used to improve the estimation of PP by ETR were selected using forward stepwise regression. According to this method, the variables DIP and PAR were selected. Due to the high correlation coefficients between DIP, DIN and DSi concentrations [23] only the variable DIP was used in the model, even though high correlation between ΔP and all nutrient concentrations were found.

A multiple linear regression was performed to estimate ΔP as a function of PAR and DIP. The result of the multiple linear regression was added to *Sim_{ETR1}* to improve the carbon incorporation estimation by ETR. The second estimation of carbon incorporation (*Sim_{ETR2}*, $P_{\text{simETR2}} = 0.2082 + 0.0496 * \ln(\text{ETR}) - (0.319 * \text{DIP}) + (0.000166 * \text{PAR})$, equation 12) based on multiple linear regression approach was in good agreement with P_{obs} and the value of the R² was high, 0.7654 (p<0.0001) (Figure 5).

2. Understanding the Relationship between Carbon Incorporation and ETR

The ratio between ETR and P_{obs} was plotted against light intensity. Each curve was fitted using equation 10. To better understand this relationship, three parameters were defined. These parameters allowed the curve of the ETR/P_{obs} vs. the light relationship to be described. R_{Max} represents the maximum value of ETR/P_{obs} estimated and E_{Rmax} the light intensity at which R_{Max} was measured. The parameter γ is the initial slope of the curve (Figure 2). The three parameters varied markedly over the data set (Table 1). R_{Max} varied from 2.54 to 85.54 mol e⁻ mol C⁻¹, E_{Rmax} varied from 0 to 4143 $\mu\text{mol photons m}^{-2} \text{ s}^{-1}$ and γ varied from -0.097 to 0.152 mol e⁻ mol C⁻¹ ($\mu\text{mol photons m}^{-2} \text{ s}^{-1}$)⁻¹.

The typology of Ward's clustering performed on R_{max}, E_{Rmax} and γ enabled the data to be divided into six groups (A, B, C, D, E and F) (Figure 6). Each group was characterized by the shape of the curve describing the relationships between the ETR/P_{obs} ratio and the light. Examples of the different shapes are shown in Figure 7.

PCA was used to highlight the link between physicochemical and biological parameters and the six curve shapes defined by Ward's clustering. The two first axes of the PCA explained more than 40% and 30% of the total inertia, respectively (Figure 8A).

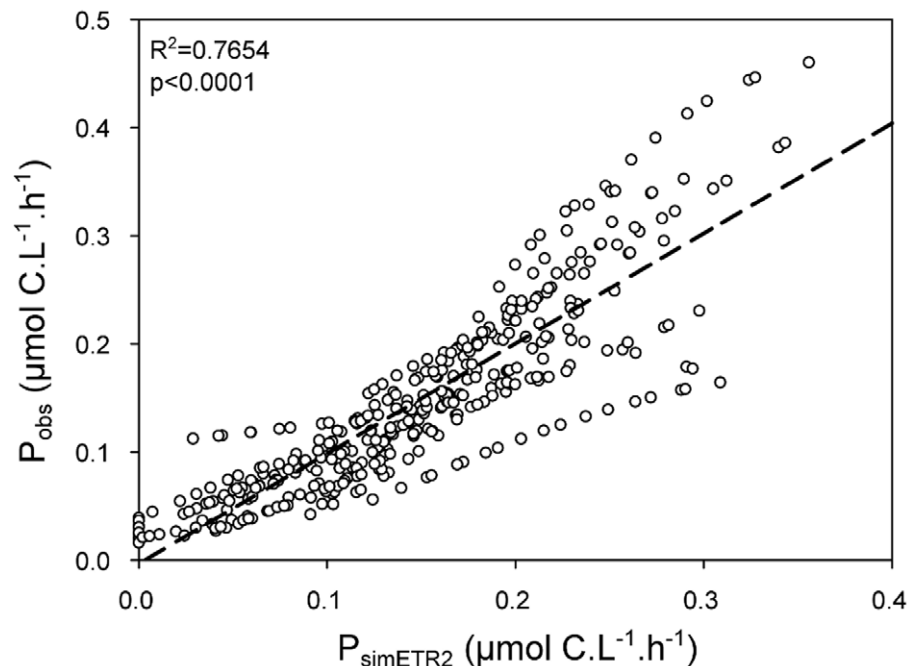


Figure 5. Observed ¹³C incorporation (P_{obs}) plotted against estimated carbon incorporation by the equation *Sim_{ETR2}*. $P_{\text{simETR2}} = 0.2082 + 0.0496 * \ln(\text{ETR}) - (0.319 * \text{DIP}) + (0.000166 * \text{PAR})$. The dotted line represents the linear regression ($P_{\text{obs}} = -0.0031 + 1.0175 * P_{\text{simETR2}}$).
doi:10.1371/journal.pone.0040284.g005

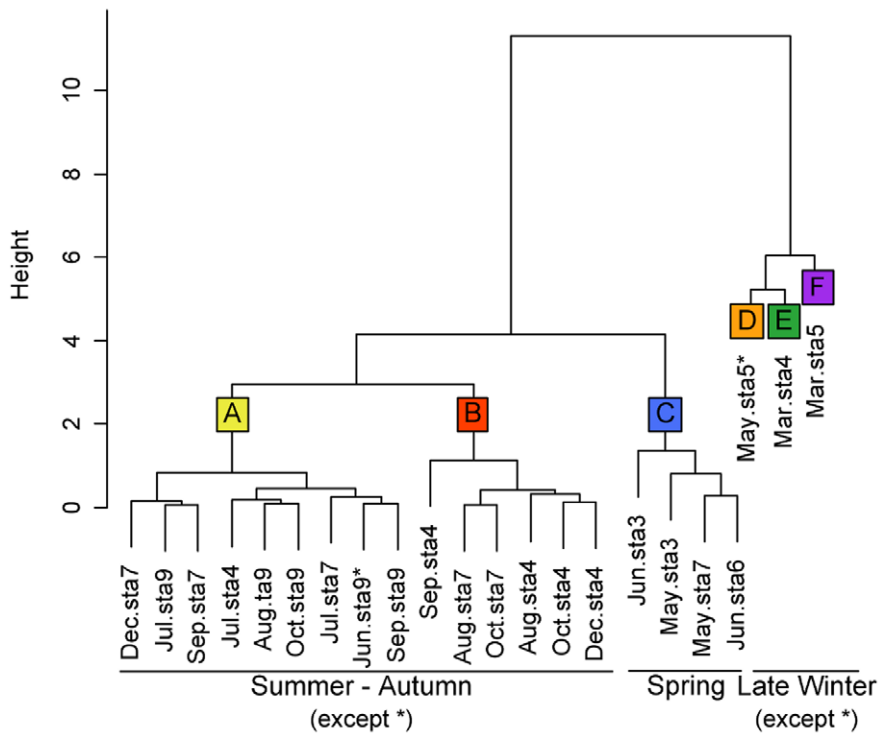


Figure 6. Tree topology obtained by Ward's clustering performed on R_{\max} , $E_{R\max}$ and γ .
doi:10.1371/journal.pone.0040284.g006

Therefore the analysis of the PCA was based on the two first axes. DIN, DIP and DSI were related to the first component whereas the biological parameters Chl a biomass, dinoflagellate:diatom ratio and SPM were related to the second component (Figure 8B). According to the factor loadings plot of the PCA and to the coefficients of correlation (data not shown), R_{\max} was positively correlated with DIP, DIN and F_v/F_m and negatively with temperature, whereas $E_{R\max}$ and γ were positively correlated with the Chl a biomass and the SPM was negatively correlated with the dinoflagellate:diatom ratio and DSI.

The sample ordination plot (Figure 8C) shows that the shape of the ETR/P_{obs} vs. light curves depended on the physicochemical and biological parameters. The six curve shapes were associated with specific environmental conditions. A high R_{\max} characterised groups E and F which were associated with high nutrient concentrations. High γ and $E_{R\max}$ characterised groups C and D, which were positively correlated with Chl a biomass, SPM and PAR_{\max} and negatively correlated with the dinoflagellate:diatom ratio and the DSI concentration. Low γ and $E_{R\max}$ generally characterized groups A and B associated with low Chl a concentrations and a high dinoflagellate:diatom ratio. Moreover, A and B were associated with the first axis mainly built by the nutrient concentrations, revealing the high influence of nutrients.

3. Estimation of the Primary Production Capacity using ETR

Carbon incorporation (P_{obs}) was measured at a low frequency (22 measurements) whereas the other parameters including PAM were measured at a high frequency (358 measurements) from November 2009 to December 2010. The paper by Napoléon et al. [23] presented the complete dataset of rETR (relative values) and the results of monitoring the dynamics of rETR throughout the year. In order to estimate PP, the Sim_{ETR2} model described above

was applied to the complete dataset from the central English Channel after the transformation of rETR data into ETR, using a_{ph} data measured during those cruises (Figure 9A). The spatiotemporal variability of a_{ph} revealed a clear seasonal pattern with higher values in winter/spring i.e. between March and July from the French coasts to the centre of the English Channel. The highest value of $5.27 \cdot 10^{-2} \text{ m}^{-1}$ was recorded in March at latitude 49.37. The lowest value of $3.46 \cdot 10^{-4} \text{ m}^{-1}$ was measured in February at latitude 50.16.

The dinoflagellate:diatom ratio remained low throughout the year of study (Figure 9B) and was related to a_{ph} . The lowest values were recorded between November 2009 and June 2010 from the French coast to the centre of the English Channel. The highest value of 11.98 was recorded in September near the French coast.

ETR_{\max} was highly variable over time and space (Figure 9C). A peak was observed between March and June on the French coast with a maximum value of $24.12 \mu\text{mol e}^{-} \text{ L}^{-1} \text{ h}^{-1}$. The minimum value of $0.34 \mu\text{mol e}^{-} \text{ L}^{-1} \text{ h}^{-1}$ was recorded in May at latitude 50.47.

The result of the conversion of the ETR_{\max} data into an estimated maximum carbon incorporation (PP_{\max}) using the Sim_{ETR2} model is shown in Figure 9D. From March to June, PP_{\max} values higher than $0.37 \mu\text{mol C L}^{-1} \text{ h}^{-1}$ were calculated from the French coast to latitude 49.71. A smaller summer peak was observed from the English coast to latitude 50.65 with PP_{\max} values higher than $0.25 \mu\text{mol C L}^{-1} \text{ h}^{-1}$. The lowest values were measured in winter.

Discussion

1. Carbon Incorporation Measurements vs. ETR

The ^{13}C method was used to estimate carbon incorporation (P_{obs}). P_{obs} measurements were then plotted against ETR measurements. A logarithmic relationship was found between

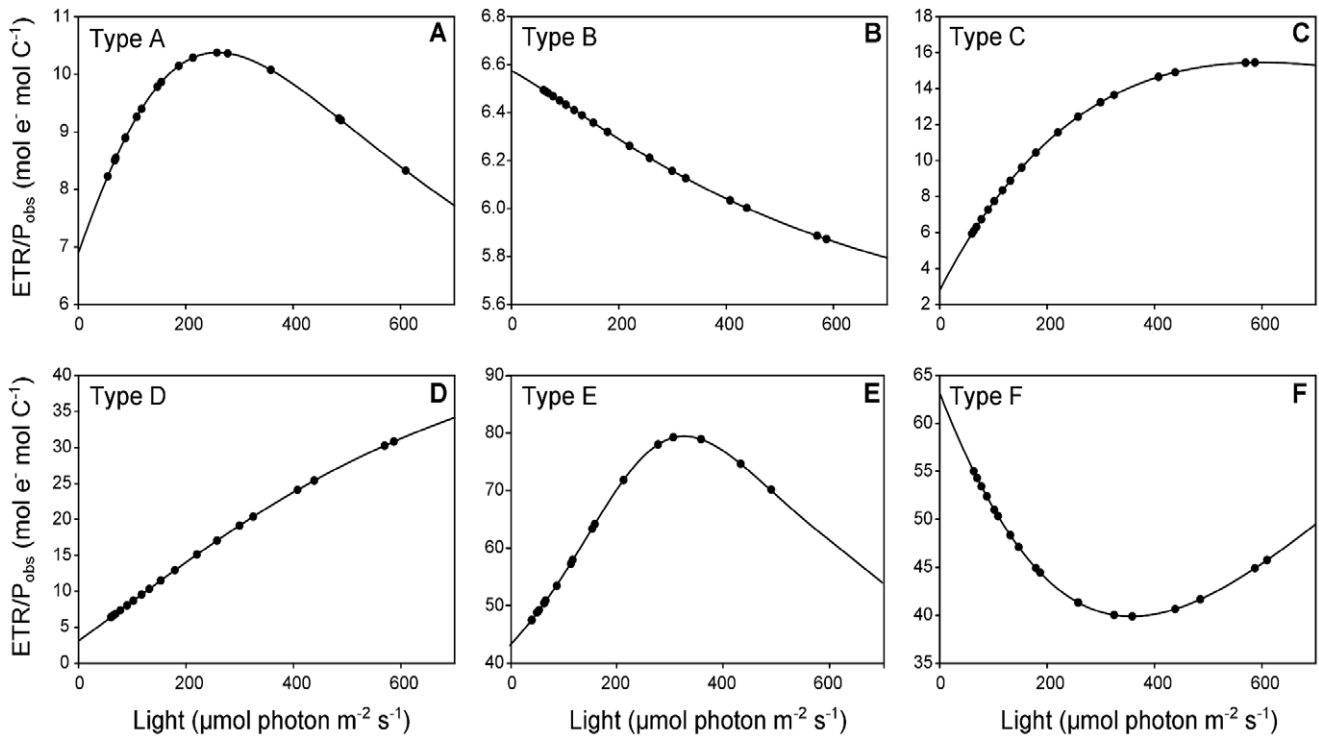


Figure 7. Relationships between the ETR/ P_{obs} ratio and light showing the different shaped curves obtained. (A) in August 2010 at station 9 corresponding to a Type A shape, (B) in October 2010 at station 7 corresponding to a Type B, (C) in June 2010 at station 6 corresponding to a Type C, (D) in May 2010 at station 5 corresponding to a Type D, (E) in March 2010 at station 4 corresponding to a Type E and (F) in March 2010 at station 5 corresponding to a Type F.
doi:10.1371/journal.pone.0040284.g007

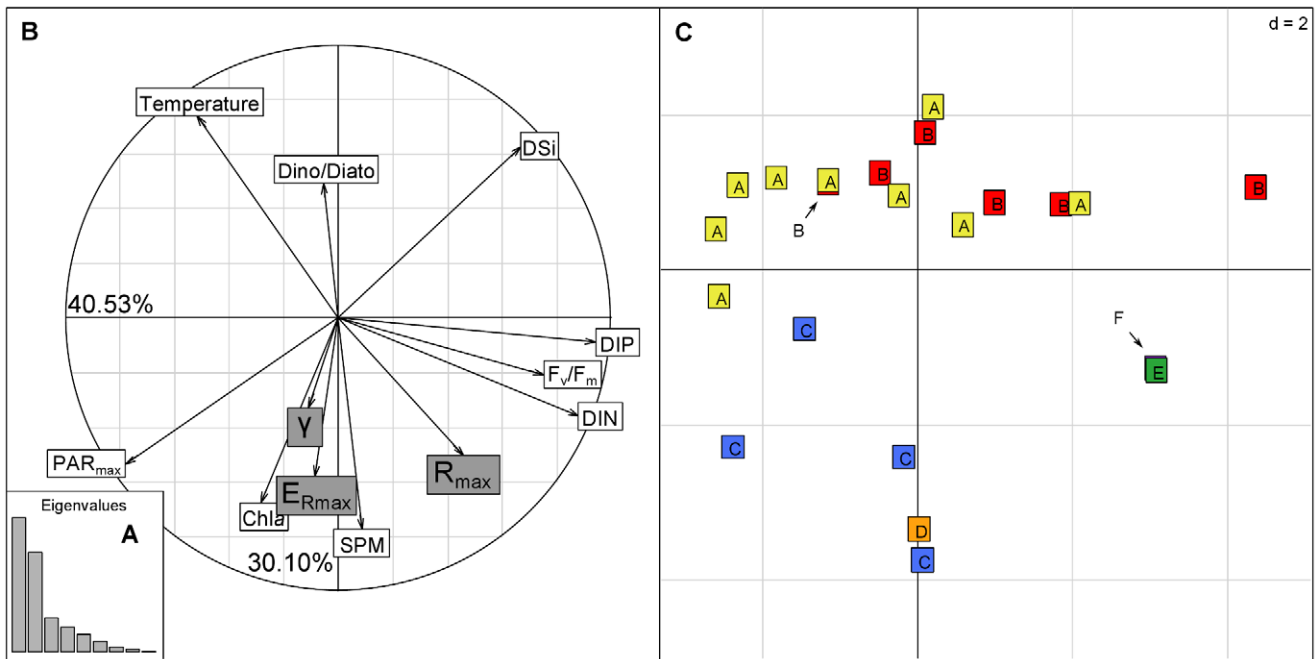


Figure 8. Principal Component Analysis highlighted the link between physicochemical and biological parameters and the 6 different curve shapes. (A) Histogram of eigenvalues, (B) Principal Component Analysis (PCA) plot of factor loadings in the plane defined by the two first axes. White labels refer to active variables and grey labels to illustrative variables, (C) Sample ordination plot. A, B, C, D, E and F refer to groups defined by Ward's clustering.
doi:10.1371/journal.pone.0040284.g008

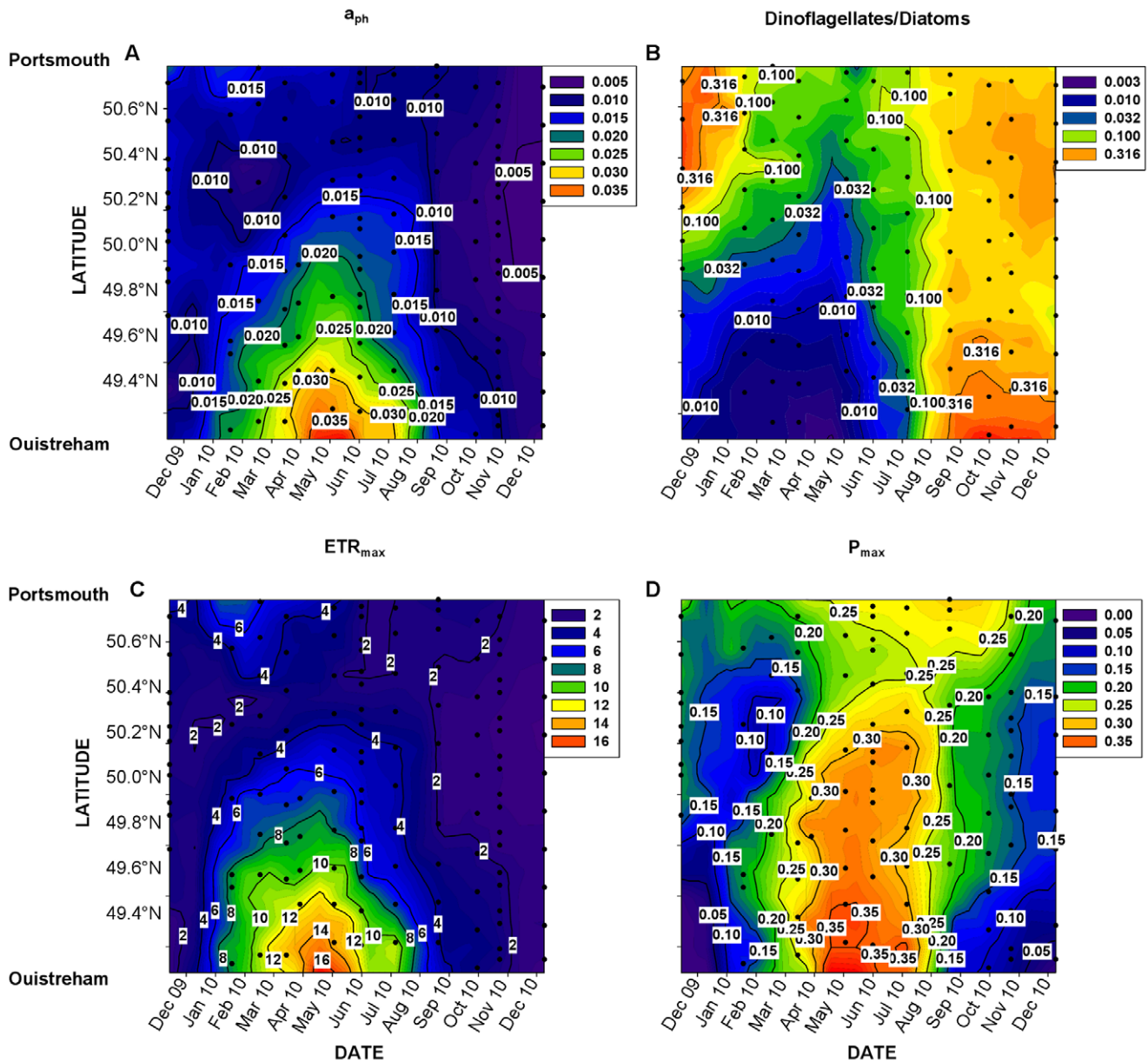


Figure 9. Latitude-time distributions of a_{ph} , the dinoflagellate:diatom ratio, ETR_{max} and P_{max} . (A) a_{ph} in m^{-1} , (B) the dinoflagellate:diatom ratio (C) ETR_{max} the maximum photosynthetic capacity (maximal electron transport rate – ETR_{max}) in $\mu mol e^{-} L^{-1} h^{-1}$ and (D) P_{max} maximum estimated carbon incorporation using the *Sim_{ETR2}* model in $\mu mol C L^{-1} h^{-1}$. doi:10.1371/journal.pone.0040284.g009

P_{obs} and ETR , with an initial slope of $0.138 mol C (mol e^{-})^{-1}$ which is in agreement with values reported in the literature [12,17]. Similar non-linear relationships between oxygen production or carbon incorporation and electron transport rates were also found in planktonic microalgae by Geel et al. [36], Flaming and Krompkamp [19], Masojedek et al. [37] and Schaeffer et al. [38].

Alternative electron sinks at high irradiance may explain such a relationship to protect the phytoplankton from photoinhibition by damage to the PSII under high irradiance. Indeed, electrons produced from the PSII are involved in the production of reducing equivalents and ATP subsequently required for carbon fixation. However, besides this linear transport of photosynthetic electrons, there are other ways for electrons cycling and divergence of electrons occurs with other reactions [39]. Several physiological

mechanisms may explain these electron sinks: photorespiration involving the oxygenase activity of the Rubisco; the Mehler reaction, which involves O_2 as the last acceptor of electrons in the PSI instead of $NADP^{+}$; nitrate reduction by nitrate reductase, which can also be an electron sink [39].

Photorespiration probably plays a minor role as shown by Geel et al. [36], Flaming and Krompkamp [19] and Claquin and al. [18]. The apparent absence of photorespiration has often been described in algae [40] and particularly in diatoms, which have an efficient CO_2 -concentration mechanism [18,41,42].

Higher Mehler activity at high irradiance can be another electron sink rather than photorespiration according to Geel et al. [36], Flaming and Krompkamp [19] and Claquin et al. [18]. This pseudocyclic electron transport can represent between 50% to

60% of the oxygen uptake stimulated by light at medium and high irradiances [18].

The reduction of nitrate can lead to a significant loss of photosynthetic electrons [43]. In diatoms, nitrate uptake and reduction occur even in the absence of metabolic demand. Under no nitrogen limitation, diatoms, which represented the largest biomass in our samples, are able to transform excess photosynthetic energy into nitrate reduction [43].

In addition, an increase in dark respiration (mitochondrial respiration) may also explain the difference between the rate of carbon fixation and ETR [19]. Indeed, mitochondrial respiration is higher in the light than in the dark [18,44,45]. Mitochondrial activity is probably limited by the concentration of substrate in the dark. In the light, the production of photosynthates probably increases mitochondrial respiration by providing more substrate for the Calvin cycle [46]. This process could thus play a role in the non-linear relationships observed between P_{obs} and ETR at high light intensities. The experiments conducted in the present study did not make it possible to define the proportion of each sink in the deviation between P_{obs} and ETR.

The relationship between P_{obs} and ETR appeared to vary as a function of physicochemical and biological parameters. The latitude-time distribution of these parameters is detailed in Napoléon et al. [23]. Nutrient concentrations and the quantum efficiency of the PSII (F_v/F_m), often used as an indicator of nutrient stress [11], were negatively correlated with ΔP , indicating overestimation of Sim_{ETR} in non limiting nutrient conditions. The absence of nutrient limitations leads to high production of photosynthetic energy and to an imbalance between the generation of energy and the energy needed for growth. The electrons sinks described above, which play a protective role, may explain this regulation. In this case, the role of the nitrate reductase can be put forward. Over the year of study, DIN varied from 0.12 to 167 $\mu\text{mol L}^{-1}$ [23]. Under high DIN concentrations, the uptake in excess of nitrate and its reduction by the nitrate reductase could have played a major role in energy overflow metabolism [12,43]. As a consequence, reduced nitrate can be released to the surrounding environment [43]. The effect of phosphate concentration, which varied from 0.06 to 1.75 $\mu\text{mol L}^{-1}$ [23], appeared to play a role but the mechanisms were not clear. Thus, the relation between carbon incorporation and ETR cannot be described by a simple relation but certainly involves many factors, especially light and nutrient variables, in modulating the relationship between P_{obs} and ETR because of the deviation at high light intensity and as a function of nutrient concentrations. The effect of nutrient limitations probably varies with the nutrient concerned [43,47] but in the present work, the strong correlation observed between all nutrients made it impossible to determine the specific effect of each individual nutrient.

According to the low correlation between ΔP and the dinoflagellate:diatom ratio, the relationship between P_{obs} and ETR did not depend on the structure of the community. However, a_{ph} , used to transform $rETR$ data into ETR data, varied considerably with species composition [29]. The effect of the species composition was consequently taken into account in the calculation of ETR.

However, caution is required here, because a high correlation does not necessarily imply a causal effect. The parameters taken into account could be good integrators of seasonality, without acting directly on the ETR vs. P_{obs} relationship.

2. Understanding the Relationship between Carbon Incorporation and ETR

The light intensity drives the relation between carbon incorporation and ETR as described above. Some authors have taken the slope coefficient and the intercept of the linear regression of the P_{obs} vs. ETR relationship into account [12,17] but none has accounted for changes in the ETR/P_{obs} ratio as a function of light. In our study, to better understand this relationship, three parameters were defined to describe changes in the ETR/P_{obs} ratio as a function of the light intensity. E_{Rmax} indicates the light intensity at which the ratio between ETR and P_{obs} reached maximum (R_{max}). γ , the initial slope expresses the efficiency of carbon fixation in moles of carbon per mole of electrons produced as a function of the light. Thus, six curve shapes were described for the whole dataset which were in accordance with the seasonal cycle e.g. shapes A and B correspond to summer and autumn data, shapes C and D correspond to spring, and shapes E and F to winter. In Barranguet and Kromkamp [12], the absence of seasonality of the conversion factor of ETR to PP was observed for microphytobenthos. On the contrary, our results highlight the importance of the seasonal cycle of the physicochemical parameters and/or biological parameters in the relationships between the ETR/P_{obs} ratio and light intensity. This can be explained by the different drivers encountered in our system versus in benthic systems.

The relationship between the ETR/P_{obs} ratio vs. light showed that the losses of electrons in other ways than the fixation of carbon increased with light intensity up to the E_{Rmax} intensity as described above. High E_{Rmax} were recorded in spring (types C and F) and low E_{Rmax} in summer and autumn (types A and B). Seasonal changes in the structure of the community may explain such variations. Glee and al. [36] showed that the light intensity at which the deviation between carbon incorporation and ETR takes place depends on the algal species and can vary from 200 to 1000 $\mu\text{mol photon m}^{-2} \text{s}^{-1}$. In our study, low dinoflagellate:diatom ratios were recorded from the end of winter to the end of spring while high values were recorded from the end of spring to the end of autumn due to an increase in the dinoflagellate biomass. Beyond the E_{Rmax} intensity, the slight decrease in the ETR/P_{obs} ratio means that the production of electrons in the PSII was affected at high light intensity, whereas dark reactions of photosynthesis were not damaged.

Low values of the parameter γ were recorded in summer and autumn (types A and B) and high values in spring (types C). Low values reveal the incapacity of the cells to respond to an increase in light and early photoinhibition, while high values show that phytoplankton cells are able to cope with the increase in electron production with light without damaging the PSII. E_{Rmax} and γ covaried because they both characterise the capacity of the phytoplankton to respond to changing light and to adapt to low or high light intensity. E_{Rmax} and γ were positively correlated with PAR_{max} , revealing a high capacity of the cells growing under high light intensity to respond to the increase in light. At high light intensity the alternative electron sinks offset the high rate of electron production. Conversely, low values of E_{Rmax} and γ reveal that high photoinhibition mechanisms came into play with an increase in light. It thus appears that photoinhibition mechanisms can occur at lower light intensities in the case of phytoplankton adapted to low light. The efflorescence of dinoflagellates was correlated with low values of E_{Rmax} and γ , revealing that dinoflagellate cells were less able to respond to changing light conditions than diatom cells [48].

R_{max} represents the highest ETR/P_{obs} preceding the occurrence of photoinhibition mechanisms. High values of R_{max} recorded in

types E and F were correlated with high nutrient concentrations and high F_v/F_m . We thus suggest that high R_{max} values reflect the high capacity of a cell to cope with an unbalance between energy production and the energy it requires for growth. Nutrient limitations could play an important role in determining cell susceptibility to photoinhibition [49]. In particular, photoinhibition is higher for cells limited by nitrogen [50]. In fact, the capacity to respond to changing light is affected by nutrient stress [20,51]. Furthermore, R_{max} was negatively correlated with temperature. These results are consistent with those of Morris and Kromkamp [17]. The slope coefficient of the ETR vs. P_{obs} relationship was negatively affected by temperature from 5°C to 20°C, which was the range of temperature recorded in our area over the year of study [23].

3. Estimation of the Primary Production Capacity in the Central English Channel

By using this approach and the *Sim_{ETR2}* model, we were able to estimate the maximum primary production (PP_{max}) in the central part of the English Channel between November 2009 and December 2010. Low frequency data of carbon incorporation measurements (P_{obs}) were combined with the high frequency data of PAM measurements detailed in Napoléon et al. [23].

The a_{ph} values allowed us to transform the $rETR_{max}$ dataset (relative unit) into ETR_{max} data. The range of a_{ph} is in accordance with those cited in the literature [30]. A seasonal variability of a_{ph} was revealed with higher values in winter/spring. The seasonality of a_{ph} depends to a great extent on the dynamics of the phytoplankton biomass [23] and is also due to the package effect [30,52] which varies as a function of photoacclimation and with the phytoplankton species. Johnsen and Sakshaug [29] showed that the values of the specific absorption cross-section (a^*) (data not shown) were higher for dinoflagellates than diatoms, which is in agreement with the high a^* values we measured during summer when the dinoflagellate:diatom ratio was high.

The levels of productivity (data not shown) estimated in the present study using the *Sim_{ETR2}* model reached values of 10 mgC mg Chla⁻¹ h⁻¹ at the beginning of summer which is in agreement with measurements made by Jouenne et al. [53], Pannard et al. [3] and Claquin et al. [51] with maximum values of 8.88, 8.48 and 17 mgC mg Chla⁻¹ h⁻¹ respectively. The dynamics was also in agreement with the results of Jouenne et al. [53] in a French estuarine bay of the English Channel (Veys Bay). The French

coastal area had a higher production rate than the English coastal area and the highest rate of production was measured from April to July whereas in the English coastal area, the rate of production was low but constant from April to the end of October. As described in Napoléon et al. [23], the French coastal area receives high freshwater inputs whereas low nutrient concentrations were recorded in the English coastal area, and this is the main explanation for the difference in dynamics between these two coastal areas (see Napoléon et al. [23] for details).

Conclusion

We have highlighted the non-linear relationship between ETR measurements and P_{obs} and underlined the importance of taking physicochemical parameters like the incident light or nutrient concentrations into account to understand and estimate PP using ETR data. By combining the two methods, we have shown that it is possible to access the high spatial and temporal dynamics of primary production.

However, we used an empirical model. To confirm the hypotheses we put forward to explain the ETR vs. P_{obs} relationship, experiments under controlled conditions are required.

The same type of approach should be used for other ecosystems to explore in more detail the parameters which control the relation between PP and ETR. In addition, extensive experiments on monoclonal cultures belonging to different phyla under different conditions are necessary to hierarchize the parameters controlling this relationship.

Acknowledgments

We thank Marie-Paule Bataillé, Liliane Fiant, Bruno Fontaine, Bertrand Le Roy, Jean-Paul Lehodey, Laurent Perez, Olivier Pierre-Duplessix, Emilie Rabiller, Virginie Raimbault and Philippe Riou for their technical assistance. We thank David Doxaran from Laboratoire Océanographique de Villefranche-sur-Mer for spectrophotometric measurements. The authors are grateful to the CREC marine station for its material assistance. The authors gratefully acknowledge officers and crew of the *Normandy-Brittany Ferries* for providing facilities for this study.

Author Contributions

Conceived and designed the experiments: PC CN. Performed the experiments: CN PC. Analyzed the data: CN PC. Contributed reagents/materials/analysis tools: CN PC. Wrote the paper: CN PC.

References

1. Pauly D, Christensen V (1995) Primary production required to sustain global fisheries. *Nature* 374: 255–257.
2. Cloern JE (1996) Phytoplankton bloom dynamics in coastal ecosystems: A review with some general lessons from sustained investigation of San Francisco Bay, California. *Reviews of Geophysics* 34: 127–168.
3. Pannard A, Claquin P, Klein C, Le Roy B, Veron B (2008) Short-term variability of the phytoplankton community in coastal ecosystem in response to physical and chemical conditions' changes. *Estuarine Coastal and Shelf Science* 80: 212–224.
4. Gaxiola-Castro G, Alvarez-Borrego S, Lavin MF, Zirino A, Najera-Martinez S (1999) Spatial variability of the photosynthetic parameters and biomass of the Gulf of California phytoplankton. *Journal of Plankton Research* 21: 231–245.
5. Platt T, Sathyendranath S, Forget MH, White GN, Caverhill C, et al. (2008) Operational estimation of primary production at large geographical scales. *Remote Sensing of Environment* 112: 3437–3448.
6. Tan SC, Shi GY (2009) Spatiotemporal variability of satellite-derived primary production in the South China Sea, 1998–2006. *Journal of Geophysical Research-Biogeosciences* 114.
7. Grangeré K, Lefebvre S, Menesguen A, Jouenne F (2009) On the interest of using field primary production data to calibrate phytoplankton rate processes in ecosystem models. *Estuarine Coastal and Shelf Science* 81: 169–178.
8. Babin M, Morel A, Gagnon R (1994) An incubator designed for extensive and sensitive measurements of phytoplankton photosynthetic parameters. *Limnology and Oceanography* 39: 694–702.
9. Savidge G, Boyd P, Pomroy A, Harbour D, Joint I (1995) Phytoplankton production and biomass estimates in the northeast Atlantic-ocean, May to June 1990. *Deep-Sea Research Part I-Oceanographic Research Papers* 42: 599–617.
10. Kromkamp JC, Forster RM (2003) The use of variable fluorescence measurements in aquatic ecosystems: differences between multiple and single turnover measuring protocols and suggested terminology. *European Journal of Phycology* 38: 103–112.
11. Parkhill JP, Maillet G, Cullen JJ (2001) Fluorescence-based maximal quantum yield for PSII as a diagnostic of nutrient stress. *Journal of Phycology* 37: 517–529.
12. Barranguet C, Kromkamp J (2000) Estimating primary production rates from photosynthetic electron transport in estuarine microphytobenthos. *Marine Ecology Progress Series* 204: 39–52.
13. Kolber Z, Falkowski PG (1993) Use of active fluorescence to estimate phytoplankton photosynthesis in-situ. *Limnology and Oceanography* 38: 1646–1665.
14. Hancke K, Hancke TB, Olsen LM, Johnsen G, Glud RN (2008) Temperature effects on microalgal photosynthesis-light responses measured by O-2 production, pulse-amplitude-modulated fluorescence, and C-14 assimilation. *Journal of Phycology* 44: 501–514.
15. Marchetti A, Sherry ND, Juneau P, Strzepek RF, Harrison PJ (2006) Phytoplankton processes during a mesoscale iron enrichment in the NE subarctic Pacific: Part III - Primary productivity. *Deep-Sea Research Part II-Tropical Studies in Oceanography* 53: 2131–2151.

16. Babin M, Morel A, Claustre H, Bricaud A, Kolber Z, et al. (1996) Nitrogen- and irradiance-dependent variations of the maximum quantum yield of carbon fixation in eutrophic, mesotrophic and oligotrophic marine systems. *Deep-Sea Research Part I-Oceanographic Research Papers* 43: 1241–1272.
17. Morris EP, Kromkamp JC (2003) Influence of temperature on the relationship between oxygen- and fluorescence-based estimates of photosynthetic parameters in a marine benthic diatom (*Cylindrotheca closterium*). *European Journal of Phycology* 38: 133–142.
18. Clauquin P, Kromkamp JC, Martin-Jezequel V (2004) Relationship between photosynthetic metabolism and cell cycle in a synchronized culture of the marine alga *Cylindrotheca fusiformis* (Bacillariophyceae). *European Journal of Phycology* 39: 33–41.
19. Flameling IA, Kromkamp J (1998) Light dependence of quantum yields for PSII charge separation and oxygen evolution in eucaryotic algae. *Limnology and Oceanography* 43: 284–297.
20. Behrenfeld MJ, Prasil O, Babin M, Bruyant F (2004) In search of a physiological basis for covariations in light-limited and light-saturated photosynthesis. *Journal of Phycology* 40: 4–25.
21. Hartig P, Wolfstein K, Lippemeier S, Colijn F (1998) Photosynthetic activity of natural microphytobenthos population measured by fluorescence (PAM) and ¹⁴C-tracer methods: a comparison. *Marine Ecology Progress Series* 166: 53–62.
22. Lefebvre S, Mouget JL, Loret P, Rosa P, Tremblin G (2007) Comparison between fluorimetry and oximetry techniques to measure photosynthesis in the diatom *Skeletonema costatum* cultivated under simulated seasonal conditions. *Journal of Photochemistry and Photobiology*: 131–139.
23. Napoleon C, Raimbault V, Fiant L, Riou P, Lefebvre S, et al. (2012). Spatiotemporal dynamics of physicochemical and photosynthetic parameters in the central English Channel. *Journal of Sea Research*. 69: 43–52.
24. Aminot A, Kérouel R (2007) Dosage automatique des nutriments dans les eaux marines. Versailles: Quae. 188 p.
25. Aminot A, Chaussepied M (1983) Manuel des analyses chimiques en milieu marin. Brest: CNEXO. 395 p.
26. Welschmeyer NA (1994) Fluorometric analysis of chlorophyll-a in the presence of chlorophyll-b and pheopigments. *Limnology and Oceanography* 39: 1985–1992.
27. Babin M, Theriault JC, Legendre L, Condal A (1993) Variations in the specific absorption-coefficient for natural phytoplankton assemblages - Impact on estimates of primary production. *Limnology and Oceanography* 38: 154–177.
28. Babin M, Stramski D, Ferrari GM, Claustre H, Bricaud A, et al. (2003) Variations in the light absorption coefficients of phytoplankton, nonalgal particles, and dissolved organic matter in coastal waters around Europe. *Journal of Geophysical Research-Oceans* 108.
29. Johnsen G, Sakshaug E (2007) Biooptical characteristics of PSII and PSI in 33 species (13 pigment groups) of marine phytoplankton, and the relevance for pulse-amplitude-modulated and fast-repetition-rate fluorometry. *Journal of Phycology* 43: 1236–1251.
30. Nelson NB, Prezelin BB, Bidigare RR (1993) Pphytoplankton light absorption and the package effect in California coastal waters. *Marine Ecology-Progress Series* 94: 217–227.
31. Schreiber U, Schliwa U, Bilger W (1986) Continuous recording of photochemical and nonphotochemical chlorophyll fluorescence quenching with a new type of modulation fluorometer. *Photosynthesis Research* 10: 51–62.
32. Genty B, Briantais JM, Baker NR (1989) The relationship between the quantum yield of photosynthetic electron transport and of quenching chlorophyll fluorescence. *Biochimica Et Biophysica Acta* 990: 87–92.
33. Juneau P, Harrison PJ (2005) Comparison by PAM fluorometry of photosynthetic activity of nine marine phytoplankton grown under identical conditions. *Photochemistry and Photobiology* 81: 649–653.
34. Hama T, Miyazaki T, Ogawa Y, Iwakuma T, Takahashi M, et al. (1983) Measurement of photosynthetic production of a marine phytoplankton population using a stable C-13 isotope. *Marine Biology* 73: 31–36.
35. Eilers PHC, Peeters JCH (1988) A model for the relationship between light-intensity and the rate of photosynthesis in phytoplankton. *Ecological Modelling* 42: 199–215.
36. Geel C, Versluis W, Snel JFH (1997) Estimation of oxygen evolution by marine phytoplankton from measurement of the efficiency of Photosystem II electron flow. *Photosynthesis Research* 51: 61–70.
37. Masojidek J, Grobbelaar JU, Pechar L, KobliZek M (2001) Photosystem II Electron Transport Rates and Oxygen Production in Natural Waterblooms of Freshwater Cyanobacteria During a Diel Cycle. *J Plankton Res* 23: 57–66.
38. Schaeffer BA, Kamykowski D, McKay L, Sinclair G, Milligan EJ (2007) A comparison of photoresponse among ten different *Karenia brevis* (Dinophyceae) isolates. *Journal of Phycology* 43: 702–714.
39. Wilhelm C, Buechel C, Fisahn J, Goss R, Jakob T, et al. (2006) The regulation of carbon and nutrient assimilation in diatoms is significantly different from green algae. *Protist* 157: 91–124.
40. Birmingham BC, Coleman JR, Colman B (1982) Measurement of photorespiration in algae. *Plant Physiology* 69: 259–262.
41. Burns BD, Beardall J (1987) Utilization of inorganic carbon by marine microalgae. *Journal of Experimental Marine Biology and Ecology* 107: 75–86.
42. Raven JA, Kubler JE, Beardall J (2000) Put out the light, and then put out the light. *Journal of the Marine Biological Association of the United Kingdom* 80: 1–25.
43. Lomas MW, Glibert PM (1999) Temperature regulation of nitrate uptake: A novel hypothesis about nitrate uptake and reduction in cool-water diatoms. *Limnology and Oceanography* 44: 556–572.
44. Peltier G, Thibault P (1985) O₂ uptake in the light in *Chlamydomonas*. *Plant Physiology* 79: 225–230.
45. Xue XP, Gauthier DA, Turpin DH, Weger HG (1996) Interactions between photosynthesis and respiration in the green alga *Chlamydomonas reinhardtii* - Characterization of light-enhanced dark respiration. *Plant Physiology* 112: 1005–1014.
46. Falkowski PG, Dubinsky Z, Santostefano G (1985) Light-enhanced dark respiration in phytoplankton. *Verhandlungen Internationale Vereinigung Limnologie* 22: 2830–2833.
47. Lippemeier S, Hartig P, Colijn F (1999) Direct impact of silicate on the photosynthetic performance of the diatom *Thalassiosira weissflogii* assessed by on- and off-line PAM fluorescence measurements. *Journal of Plankton Research* 21: 269–283.
48. Reynolds C (2006) *The ecology of phytoplankton*. Cambridge: Cambridge University Press. 535 p.
49. Prezelin BB, Samuelson G, Matlick HA (1986) Photosystem II photoinhibition and altered kinetics of photosynthesis during nutrient-dependent highlight photoadaptation in *Gonyaulax Polyedra*. *Marine Biology* 93: 1–12.
50. Kolber Z, Zehr J, Falkowski PG (1988) Effects of growth irradiance and nitrogen limitation on photosynthetic energy conversion in photosystem II. *Plant Physiology* 88: 923–929.
51. Clauquin P, Longphuir SN, Fouillaron P, Huonnic P, Ragueneau O, et al. (2010) Effects of simulated benthic fluxes on phytoplankton dynamic and photosynthetic parameters in a mesocosm experiment (Bay of Brest, France). *Estuarine Coastal and Shelf Science* 86: 93–101.
52. Falkowski PG, Raven JA (2007) *Aquatic Photosynthesis*. Princeton: Princeton University Press.
53. Jouenne F, Lefebvre S, Veron B, Lagadeuc Y (2007) Phytoplankton community structure and primary production in small intertidal estuarine-bay ecosystem (eastern English Channel, France). *Marine Biology* 151: 805–825.